


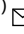

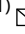






## Hybrid machine learning for flood prediction: comparing CHIRPS satellite and ground station data

Agustina Rachmawardani<sup>1), 2)</sup>  , Budhy Kurniawan\*<sup>1)</sup>  , Sastra Kusuma Wijaya<sup>1)</sup>  ,  
Ardhasena Sopaheluwakan<sup>3), 4)</sup>  , Marzuki Sinambela<sup>2)</sup>  

<sup>1)</sup> Universitas Indonesia, Faculty of Mathematics and Natural Sciences, Department of Physics, Building F, Pondok Cina, Beji District, Depok City 16424, Indonesia

<sup>2)</sup> State College of Meteorology, Climatology and Geophysics, Meteorology Street, No 5, Tanah Tinggi Sub-district, Tangerang District, Tangerang City, Banten 15119, Indonesia

<sup>3)</sup> Indonesia's Meteorological, Climatological, and Geophysical Agency, Angkasa 1 No 2 street, Kemayoran, Central Jakarta, DKI Jakarta 10720, Indonesia

<sup>4)</sup> World Meteorological Organization (WMO), 7bis, avenue de la Paix, CH-1211 Geneva 2, Switzerland

\* Corresponding author

RECEIVED 29.09.2024

ACCEPTED 15.11.2024

AVAILABLE ONLINE 23.02.2025

**Abstract:** Flooding in Jakarta is a multifaceted issue influenced by a combination of geographical, social, economic, and environmental factors. This study focuses on predicting floods by comparing automatic rain gauge (ARG) ground station data and Climate Hazards Group InfraRed Precipitation (CHIRPS) satellite data using the Adaptive Neurofuzzy Inference System (ANFIS) integrated with principal component analysis (PCA). The dataset includes precipitation measurements from both ARG and CHIRPS along with water level data spanning from 2014 to 2020. ARG provides precise local rainfall data, while CHIRPS offers extensive regional precipitation coverage. To enhance data quality, preprocessing techniques such as mean imputation, data normalisation, and the interquartile range (*IQR*) method were employed. The ANFIS-PCA model, which integrates fuzzy logic and neural network training, was applied using an 80:20 split for training and validation. When trained with ARG ground station data and water level measurements, the ANFIS-PCA model demonstrated superior accuracy, achieving a root mean square error (*RMSE*) of 0.13, mean absolute error (*MAE*) of 0.12, and  $R^2$  of 0.82. In contrast, the ANFIS model without PCA yielded higher errors, with *RMSE* 6.3, *MAE* 6.2, and  $R^2$  0.74. Training with CHIRPS satellite data resulted in significantly higher errors (*RMSE* 30.14, *MAE* 24.05,  $R^2$  0.42). These findings underscore the superiority of ground-based measurements for flood prediction, given the reduced precision and higher susceptibility to errors in satellite-derived data. While CHIRPS satellite data offers broader spatial coverage, its limitation in precision and higher susceptibility to errors reduce its effectiveness for accurate flood prediction.

**Keywords:** adaptive neuro-fuzzy inference system, flood prediction, machine learning, rainfall, satellite data, water level

### INTRODUCTION

Flooding is one of the most frequent natural disasters in Asia. Indonesia, particularly the state capital of Jakarta, is one of the Asian countries that experiences the highest flood impacts. Jakarta has endured multiple significant floods in the twenty-first century, including in 2002, 2007, 2013, 2015, and 2020. The

floods of 2007 were considered a national disaster, resulting in losses of USD 565 mln (Bennett *et al.*, 2023). Severe precipitation in Jakarta and nearby urban areas from 17–19 January 2013 resulted in extensive flooding, leading to the destruction of 98,000 residences, displacement of 40,000 individuals, and losing 20 lives. The estimated total cost of the damage amounts to USD 775 mln (Priyambodoho *et al.*, 2021). Urban areas are particularly

vulnerable to natural disasters as they affect buildings and essential infrastructure, such as bridges, drainage systems, and power stations (Hassan, Joseph and Abubakar, 2024). Additionally, flooding also leads to lower productivity and fewer business opportunities.

Flood forecasting has traditionally relied on data from ground-based meteorological stations, which provide accurate and localized precipitation measurements. However, a major limitation of ground station data is its limited spatial coverage, particularly in rural areas or regions lacking a comprehensive monitoring network. In many developing countries, ground stations are sparsely distributed, leading to substantial gaps in the data required for reliable flood forecasting (Helmi *et al.*, 2024). To address these limitations, satellite-based precipitation data has become an increasingly valuable tool for flood prediction. Among the most widely used satellite datasets is CHIRPS, which integrates satellite imagery with terrestrial observations to produce near-global precipitation estimates at a 0.05° (~5 km) resolution, ensuring extensive spatial coverage. CHIRPS is particularly beneficial in regions with limited or nonexistent ground station data (Du *et al.*, 2024).

Machine learning (ML) provides a robust approach to flood prediction by integrating multiple data sources (Amiri *et al.*, 2024). These models efficiently process large volumes of diverse data, identifying complex patterns that traditional statistical approaches may miss. ML models are particularly effective for short-term flood prediction, as they can be trained on historical data and utilized for real-time predictions based on current conditions (Szelağ *et al.*, 2024). There are several examples demonstrating how machine learning is applied to mitigate flooding. For instance, ML models trained on historical data, such as rainfall, river flow, and satellite imagery, can provide early warnings, thereby enhancing preparedness and response efforts (Rashidi Shikhteymour *et al.*, 2023). Furthermore, ML algorithms analyse real-time data from sensors and satellite imagery to monitor floods closely, facilitating early detection and accelerating response efforts (Antzoulatos *et al.*, 2022). Additionally, these models assist in identifying flood-prone areas, informing decision-making processes for risk management (Dong *et al.*, 2021). Research conducted by Rudra and Sarkar (2023) elucidates the application of ML in modelling intricate hydrological systems, specifically floods using algorithms such as artificial neural networks (ANN) (Santos *et al.*, 2023), neuro-fuzzy (Bensaid *et al.*, 2024), multiple linear regression (MLR) (Youssef *et al.*, 2023), and regression vector support (SVR) (Azi *et al.*, 2024). Furthermore, incorporating hybridization with other machine learning methods, soft computing approaches, numerical simulations, and/or physical models holds significant potential for improving the performance of machine learning (Al-Areeq *et al.*, 2024).

Recent research has employed an Adaptive Neuro Fuzzy Inference System (ANFIS) algorithm for their modelling purposes. Samantaray *et al.* (2023) developed a novel model for predicting river flood discharge using an improved ANFIS combined with a hybrid optimization approach that integrates particle swarm optimization (PSO) and slime mould algorithm (SMA). Similarly, Ahmadi and Moradinia (2024) used Hybrid ANFIS-ACO Model, which combines the Adaptive Neuro-Fuzzy Inference System (ANFIS) with ant colony optimisation (ACO) to enhance the accuracy of flood hydrograph estimation. This hybrid approach aims to improve flood forecasting, particularly in

regions highly vulnerable to flooding. Navale and Mhaske, (2023) concluded that the ANFIS model significantly outperforms the ANN model in predicting groundwater levels in the Prav's superior accuracy and better handling of complex, nonlinear relationships. Sahoo, Samantaray, and Paul (2021) demonstrated that hybrid models, such as ANFIS-PSO and ANFIS-SMA, significantly outperform standalone models like SVM and ANN. Islam *et al.* (2023) employed ANN, fuzzy logic (FL), and random forest (RF, both as standalone models and in hybrid ensemble forms. These models were used to predict flood susceptibility by processing remote sensing data and geographical factors. Technological advances in remote sensing have significantly contributed to various aspects of flood management. More precise and real-time flood detection enables faster and more effective warning system (Rachmawardani *et al.*, 2022).

This research focuses on designing a flood early warning system that employs an ANFIS-based hybrid Machine Learning method to mitigate flood disasters. An effective method to address flooding is constructing an advanced early warning system that promptly alerts individuals about impending disasters. The primary goal of this early warning system is to reduce flood damage by providing timely and accurate information. Flood early warning systems aim to enhance Indonesia's ability to withstand disasters and encourage sustainable development by providing necessary preparations and flood mitigation measures.

## MATERIALS AND METHODS

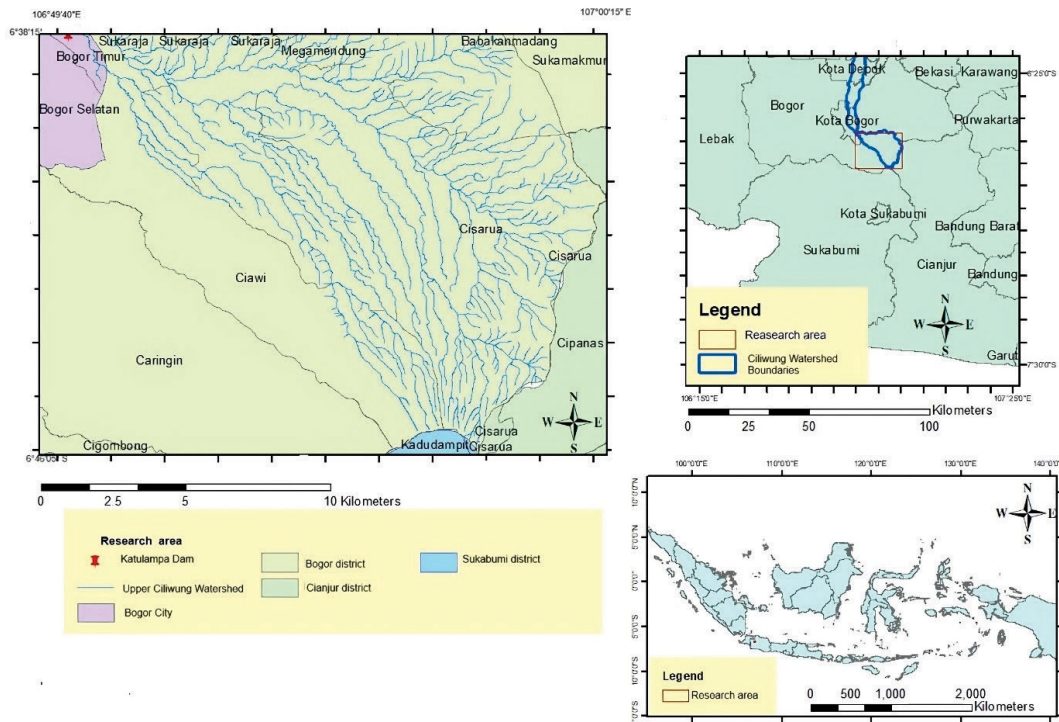
### STUDY AREA

The Upper Ciliwung River Basin plays a crucial role in contributing to flooding in Jakarta, primarily due to its complex topography and geographic characteristics. This basin serves as a major source of precipitation runoff from the surrounding mountainous areas, which flows into Jakarta through the Ciliwung River, one of the city's primary watercourses. However, the river's limited capacity to manage large volumes of water during intense rainfall increases the likelihood of flooding in urban Jakarta (Zein, Anggraheni and Yahya, 2023). Furthermore, Jakarta's location in a low-lying and predominantly flat basin exacerbates its vulnerability to flooding.

The Ciliwung Upper River Flow Area (Fig. 1) is located in two districts of West Java Province: Bogor District and Bogor City. It is one of 13 watersheds in critical condition due to land use changes (Saridewi and Fauzi, 2019). The total area of watersheds in the Upper Ciliwung from upstream to downstream is approximately 36.839 ha, while the Upper Ciliwung Watershed has an area of 15.101 ha. Consequently, the Ciliwung watersheds in upstream areas occupy 40.18% of the total surface area of the Ciliwung DAS. The location coordinates are 106°49'40"–107°00'15" E and 6°38'15"–6°46'05" S (Indriastuti, 2016).

### DATA SOURCE

The initial dataset for flood prediction research comprises water level data from the Ciliwung Watershed. This dataset includes water level measurements from the Katulampa station, spanning the period from 2014 to 2020. The data is accessible through the



**Fig. 1.** Geographic location of flood prediction modelling; source: own elaboration based on: CHIRPS spatial data and Indonesian topographic maps

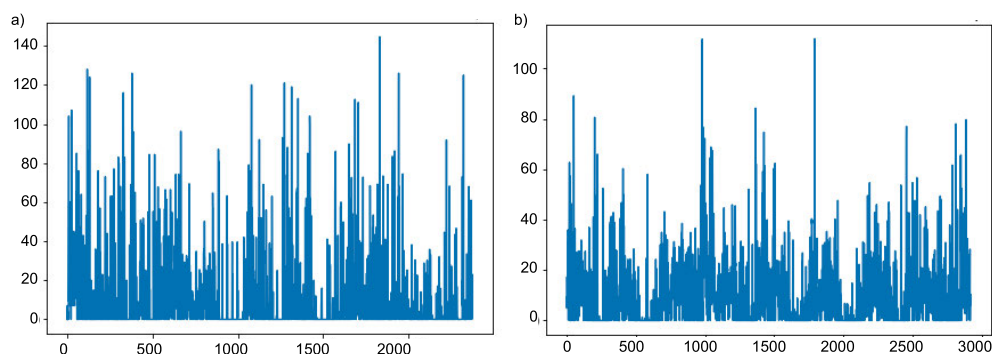
official website <https://pantaubanjir.jakarta.go.id/>, maintained by the Jakarta government. The “Pantau Banjir Jakarta” platform provides real-time monitoring and information on flood conditions in the city. Among its key features is the real-time tracking of water levels.

Rainfall data from automatic rain gauge (ARG) ground stations, specifically from the Katulampa Bogor area, were collected for the Upper Ciliwung River Basin between 2014 and 2020. These data were sourced from the BMKG website ([awscenter@bmgk.go.id](mailto:awscenter@bmgk.go.id), BMKG). In addition to ground station data, satellite rainfall data were obtained from the Climate Hazards Group InfraRed Precipitation with Station (CHIRPS) satellite for the same period. The CHIRPS dataset utilises advanced interpolation techniques and high-resolution, long-term precipitation estimates derived from infrared cold cloud duration (CCD) measurements (Sulugodu and Deka, 2019). The CHIRPS dataset was retrieved from the Climate Engine platform, an online tool designed to access, visualise, and analyse high-resolution climate and environmental

data (Wang *et al.*, 2021). The dataset about flood events in the Jakarta region from 2014 to 2020 is identified as the output data for this analysis and is available through the Jakarta Open Data portal. This project, implemented by the Jakarta government, aims to improve public access to various urban datasets. A notable example of such a dataset is the annual flood incident recap, which offers comprehensive information on flood occurrences in Jakarta. The dataset includes many data points, such as the frequency of flood incidents, the impacted regions, and other relevant statistics for each year.

#### PRE-EVALUATION OF INPUT DATA

Daily rainfall data collected from the ARG station at Katulampa and CHIRPS satellite data, covering the period from 2014 to 2020 are presented in Figure 2. This time series captures the variation in daily precipitation levels, with noticeable fluctuations reflecting seasonal rainfall patterns. Peaks in the graph indicate days with



**Fig. 2.** Daily rainfall data from: a) automatic rain gauge (ARG Katulampa), b) Climate Hazards Group InfraRed Precipitation (CHIRPS); source: own elaboration

high rainfall intensity, while lower values represent dry or low-rainfall periods.

Both the ARG Katulampa and CHIRPS datasets are aggregated at a daily time step, with rainfall measured in millimetres per day.

Table 1 presents the accumulated rainfall for ARG Katulampa and CHIRPS datasets during the training period (2014–2018) and the validation period (2018–2020). The table shows that CHIRPS consistently records higher rainfall totals than ARG Katulampa for both periods. During the training period, the total rainfall measured by CHIRPS was 19,702.22 mm, compared to 15,852.4 mm recorded by ARG, representing approximately 24% higher rainfall. Similarly, in the validation period, CHIRPS recorded 10,878.45 mm, while ARG recorded 8,849.9 mm, indicating a difference of 23%. This difference reflects the spatial nature of CHIRPS, which captures rainfall over a larger area, including upstream and surrounding regions, whereas ARG Katulampa records rainfall at a single point. The results in Table 1 indicate that while both datasets follow similar trends, CHIRPS consistently captures higher cumulative values, likely due to its broader spatial coverage.

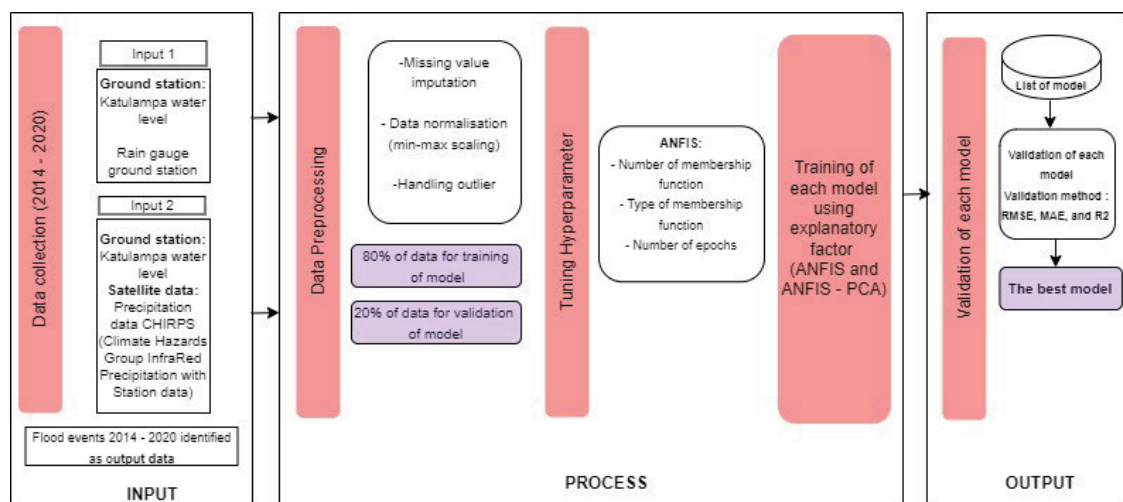
**Table 1.** Accumulated rainfall for automatic rain gauge (ARG) Katulampa and Climate Hazards Group InfraRed Precipitation (CHIRPS) during training and validation periods

Period	ARG Katulampa	CHIRPS
Training period (2014–2018)	15852.4	19702.22
Validation period (2018–2020)	8849.9	10878.45

Source: own elaboration.

## STUDY METHODS

The methodology of this study is structured into several essential phases: data collection, preprocessing, hyperparameter tuning, developing models, and performance evaluation. Each phase is critical in ensuring the precision and robustness of the flood prediction model. The subsequent sections provide a comprehensive explanation of the processes involved in each phase (Fig. 3).



**Fig. 3.** The flowchart of the research; CHIRPS = Climate Hazards Group InfraRed Precipitation, ANFIS = Adaptive Neurofuzzy Inference System, PCA = principal component analysis, source: own elaboration

## Data collection

The first phase, data collection, involves acquiring key input variables influencing flood events. The principal inputs originate from two essential sources. The first is ground station data from the Katulampa water level and a rain gauge station, providing localised hydrological measurements essential for understanding real-time water levels. The second source includes additional ground-based Katulampa water level data and CHIRPS, which offers comprehensive precipitation data, particularly in areas lacking sufficient ground measurements. CHIRPS data includes temporal resolutions at the daily, pentad, and monthly levels (Shahid *et al.*, 2021). The flood events recorded between 2014 and 2020 serve as the output for the analysis.

## Preprocessing

The next step is data preprocessing, which is essential for preparing raw data for analysis and modelling. This process involves several methods, such as missing value imputation, data normalisation, and handling outliers, to clean and transform the data, ensuring that data is appropriate for machine learning algorithms. Missing values in datasets are a common problem that can be solved via missing value imputation using the dataset mean (Gabr, Helmy and Elzanfaly, 2023). The equation for mean imputation involves calculating the mean of the observed (non-missing) values in the dataset and then replacing each missing value with this calculated mean (see Equation 1).

- The mean of observed value:

$$\bar{x} = \frac{1}{N - M} \sum_{j=1}^N (x_j) \quad (1)$$

where:  $N$  = the total number of observations in the dataset,  $M$  = the number of missing values.

The sum  $\sum_{j=1}^N (x_j)$  includes only the non-missing values.

- Impute the missing values:

$$x_i = \begin{cases} x_i, & \text{if } x_i \text{ is not missing} \\ \bar{x} & \text{if } x_i \text{ is missing} \end{cases} \quad (2)$$

The formula for mean imputation involves calculating the mean  $\bar{x}$  of all non-missing values and then substituting each

missing value with this calculated mean (García-Laencina *et al.*, 2010; Buuren van and Groothuis-Oudshoorn, 2011).

- Data normalisation (min-max normalisation)

Data normalisation is the process of standardising data to ensure consistency and comparability. Databases organise data to reduce redundancy and improve integrity by dividing it into related tables. In statistics and machine learning, normalisation adjusts data to a common scale or range, making it easier to analyse or improve algorithm performance (Singh and Singh, 2020; Shantal, Othman and Bakar, 2023).

$$x' = \frac{x - x_{\min}}{x_{\max} - x_{\min}} \quad (3)$$

where:  $x$  = original value,  $x_{\min}$  = minimum value of the feature and  $x_{\max}$  = maximum value of the feature.

- Remove outlier

The next step is to remove any outliers. The dataset is preprocessed using the interquartile range (*IQR*) approach. The *IQR* is a statistical measure to identify data irregularities or outliers. It entails dividing the data into four equal parts using the *Q1*, *Q2*, and *Q3* quartile ranges (Cho, Park and Kim, 2022). The *IQR* is calculated by subtracting the first quartile (*Q1*) from the third quartile, e.g. (*Q3*) (*Q3* - *Q1*). Outliers can be categorised into lower and upper outliers (Shabbir and Ahmed, 2022). The calculations for identifying these outliers are as follows:

- lower quartile 1 outlier =  $Q1 - 1.5IQR$
- upper quartile 1 outlier =  $Q3 + 1.5IQR$
- lower quartile 3 outlier =  $Q1 - 3IQR$
- upper quartile 3 outlier =  $Q3 + 3IQR$  (Buuren van and Groothuis-Oudshoorn, 2011).

The data will be analysed, including correcting missing values, normalising data, and treating outliers. Once the dataset has been processed, it will be utilised as input data. Next, the input data will be split into an 80:20 ratio, with 80% of the data used for training and 20% used for validation.

### Hyperparameter tuning

The third stage entails hyperparameter tuning, a crucial process for enhancing the model's performance. The model employed in this study is the Adaptive Neuro-Fuzzy Inference System (ANFIS), a hybrid framework that combines neural networks with fuzzy logic (Ansari *et al.*, 2021). The tuning process entails

modifying essential parameters of the ANFIS model to enhance its predictive performance. The parameters include the number of membership functions that delineate the mapping of inputs to membership values in fuzzy logic and the type of membership functions that define the shape and characteristics of these mappings (e.g., triangular, Gaussian). The fourth parameter, the learning rate, regulates the pace at which the model modifies its parameters during training. The parameter must be carefully selected to ensure effective convergence without overfitting (Srilakshmi *et al.*, 2024).

### Developing models

Once the hyperparameters have been tuned, the model is trained using the pre-processed data. The flowchart illustrates two model configurations: ANFIS and ANFIS combined with PCA. ANFIS is a commonly used machine learning model for complex systems, such as flood prediction, as it integrates the learning capability of neural networks with the decision-making processes of fuzzy logic (Jang, 1993; Hoshino *et al.*, 2024). The GENFIS1 is employed to generate a Sugeno-type Fuzzy Inference System (FIS) using grid partitioning, systematically creating fuzzy rules by combining all possible input membership functions. This method is particularly effective for systems with a limited number of inputs, as it ensures a comprehensive representation of the input space and captures all potential interactions between variables. However, while GENFIS1 is well-suited to smaller models requiring detailed rule generation, it can become computationally demanding for larger systems with many inputs, as the number of rules increases exponentially with each additional variable (Sarkar *et al.*, 2021). In the second model configuration, PCA is applied to reduce the dimensionality of the input data. By identifying and retaining only the most significant features, PCA helps simplify the model and improve computational efficiency without sacrificing accuracy (Karamizadeh *et al.*, 2013). The two models – ANFIS and ANFIS-PCA – are trained on the preprocessed dataset, with each aiming to generate the most accurate predictions of flood events. The architecture of the ANFIS model is depicted in Figure 4 (Pishnamazi *et al.*, 2020).

### Performance evaluation

The final stage of the process is model validation, where the trained models are assessed for their predictive performance. The ANFIS model's accuracy was evaluated using several well-

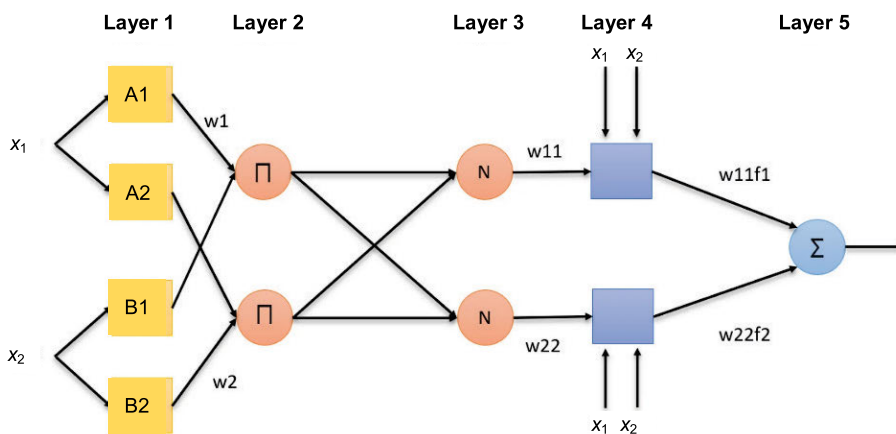


Fig. 4. Structure of the Adaptive Neuro-fuzzy Inference System model; source: Pishnamazi *et al.*, 2020, modified

established metrics: root mean squared error (*RMSE*), mean absolute error (*MAE*), and *R*-squared ( $R^2$ ), all of which are widely used for evaluating prediction models (Ly *et al.*, 2019).

The *RMSE*, defined in Equation (1), measures the square root of the average squared differences between predicted and actual values. Due to its sensitivity to larger errors, it serves as an effective metric for evaluating overall prediction accuracy (Llovo, Mosqueira and Vidal, 2018). The *MAE*, as shown in Equation (2), calculates the average absolute differences between predicted and observed values, providing a simpler interpretation of prediction errors without emphasising large errors (Günel, 2024). Additionally,  $R^2$ , detailed in Equation (3), measures how much of the variance in the observed data is explained by the model, with values closer to 1 indicating a better fit.

$$RMSE = \sqrt{\frac{1}{n} \sum_{i=1}^n (y_i - \bar{y}_i)^2} \quad (4)$$

$$MAE = \frac{1}{n} \sum_{i=1}^n |y_i - \bar{y}_i| \quad (5)$$

$$R^2 = 1 - \frac{\sum_{i=1}^n (y_i - \bar{y}_i)^2}{\sum_{i=1}^n (y_i - \bar{y})^2} \quad (6)$$

where:  $y_i$  = actual observed value for the  $i$ -th data point,  $\bar{y}_i$  = predicted value for the  $i$ -th data point,  $\bar{y}$  = mean (average) of the observed values ( $y_i$ ),  $n$  = total number of observations.

## RESULTS AND DISCUSSION

### RESULTS

#### Data description

Ensuring the integrity and correctness of transformer data through the data cleansing process is critical for producing trustworthy study results (Maharana, Mondal and Nemade, 2022). The first step is to eliminate any missing values, ensuring that only complete data is accessible for examination. Subsequently, certain criteria are employed to further refine the dataset

by excluding any negative or zero values in crucial measurement fields, retaining only pertinent data. Outliers are identified by calculating the first quartile ( $Q1$ ) and third quartile ( $Q3$ ), which facilitates the computation of the *IQR* to signal values that deviate significantly from the predicted range for further examination. The thresholds for defining outliers are set at 1.5 times the *IQR* beyond the first quartile ( $Q1$ ) and third quartile ( $Q3$ ). Specifically, any value below  $Q1 - 1.5IQR$  or above  $Q3 + 1.5IQR$  is considered an outlier. The data cleansing technique guarantees high-quality datasets devoid of anomalies that could compromise the validity of the study's results. Following preprocessing, the dataset has been meticulously cleansed by removing missing values, filtering out invalid data (negative or zero values), and identifying outliers using the *IQR* method. This ensures the dataset is accurate, complete, and free from anomalies for reliable analysis. Figures 5 and 6 are the datasets after applying the preprocessing steps outlined.

The histogram for ARG data exhibits a significant concentration of rainfall values close to zero, with a rapid decrease as precipitation rises, suggesting that the majority of rainfall events recorded by the ARG system are mild to moderate. The boxplot highlights the presence of numerous outliers, further supporting this observation. These outliers represent extreme rainfall events, with values exceeding 5 mm and some even reaching beyond 20 mm. The *IQR* is limited, indicating that most rainfall occurs between 0 and around 4 mm. On the other hand, the CHIRPS satellite data in Figure 6 exhibits a more uniformly distributed rainfall pattern across a broader range of values, as demonstrated by its histogram. In contrast to ARG, the distribution indicates that CHIRPS encompasses a broader range of precipitation events, from light to heavy rainfall, with fewer peaks at minimal precipitation values. The CHIRPS boxplot confirms this observation, displaying a broader interquartile range, generally between 5 and 20 mm, with a smaller percentage of outliers. This means that heavy rain events happen less frequently or are smoothed out in satellite data. The highest values reach about 40 mm, indicating that CHIRPS can record heavier rain events, though not as precisely as the ground-based ARG measurements.

The histogram and boxplot for the water level data (*lvl*) data both provide insights into its distribution and variability depicted in Figure 7.

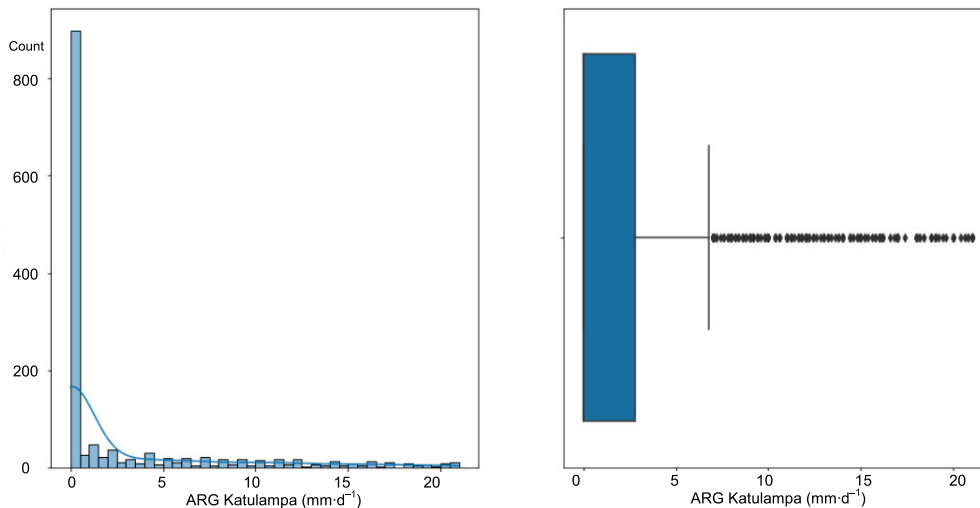
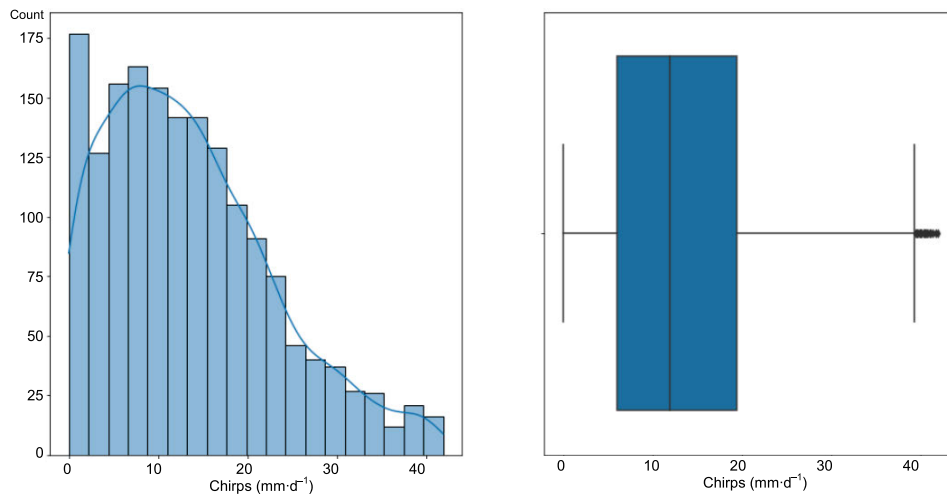
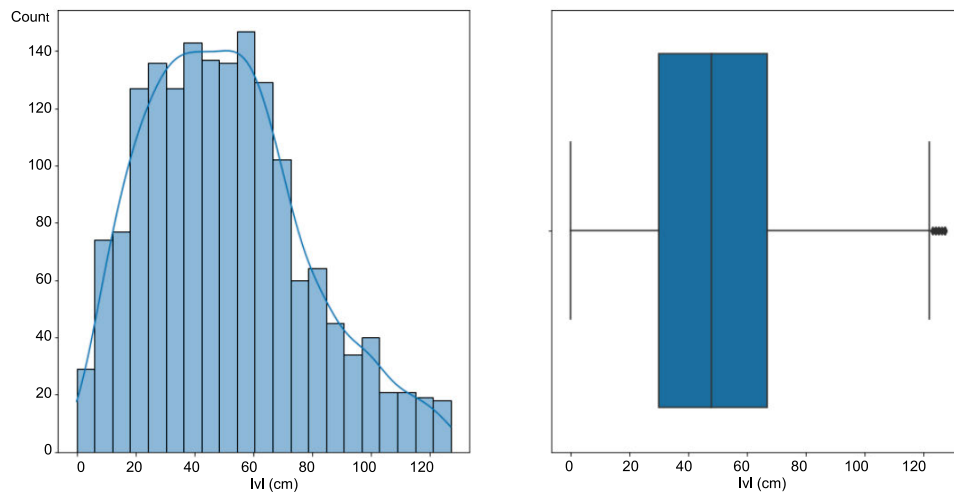


Fig. 5. The histogram and boxplot of rainfall for automatic rain gauge (ARG) Katulampa data; source: own study



**Fig. 6.** The histogram and boxplot of Climate Hazards Group InfraRed Precipitation (CHIRPS) data; source: own study



**Fig. 7.** The histogram and boxplot of water level (lvl) data; source: own study

The histogram shows that most of the level values fall between 30 and 80, indicating a concentration of data in this range. The data appears to follow a near-normal distribution but is slightly skewed to the right, with fewer occurrences of extremely high level values. The peak of the histogram is around 60–70, indicating that these values are the most common. The boxplot further confirms this distribution, with the *IQR* extending from approximately 40–80, showing where the middle 50% of the data lies. The median value, which is around 60, divides the dataset into two halves. Additionally, the boxplot reveals a few outliers beyond 120, suggesting some extreme values in the dataset that occur infrequently.

#### ANFIS training and validation result with CHIRPS satellite data

The performance of the ANFIS model applied to the CHIRPS dataset was evaluated using various configurations of membership functions (MF), MF shapes, and epochs, with distinct results obtained for both training and validation phases. The focus of this analysis is to assess how hyperparameter tuning, particularly the selection of the membership function, MF shape, and the number of epochs, influences the model's accuracy in predicting flood-related parameters.

#### Training phase

The model's performance under various configurations of membership functions is summarized in Table 2. The changes in these configurations significantly affect the model's accuracy, as reflected in the *RMSE*, *MAE*, and  $R^2$  values.

Initially, with a 2-2 Generalised Bell (Gbell MF) and 50 epochs, the model achieves an *RMSE* of 33.7, an *MAE* of 25.27, and an  $R^2$  value of 0.37. However, increasing the complexity

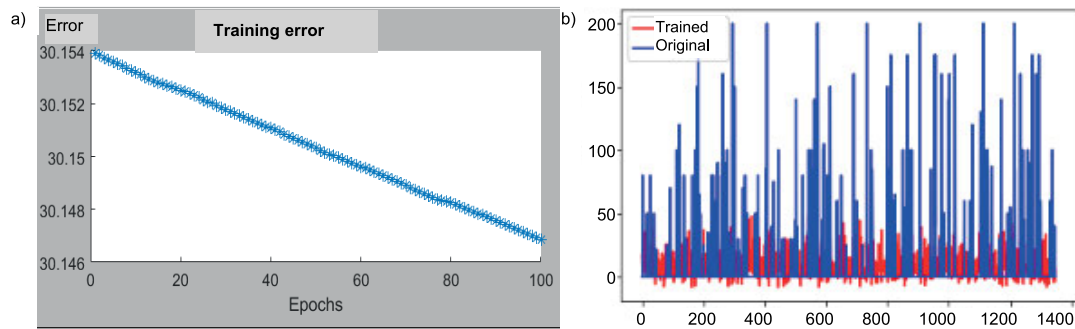
**Table 2.** Climate Hazards Group InfraRed Precipitation training data performance with varying parameter

Epoch	MF	Shape	Training data		
			<i>RMSE</i>	<i>MAE</i>	$R^2$
50	2-2	Gbell MF	33.7	25.27	0.37
100	3-3	Gbell MF	32.9	24.67	0.36
100	3-3	Gauss MF	31.35	25.16	0.41
100	4-4	Gauss MF	30.14	24.05	0.42

Explanations: MF = membership function, *RMSE* = root mean square error, *MAE* = mean absolute error,  $R^2$  = determination coefficient. Source: own study.

to 3-3 MFs and 100 epochs results in a slight decrease in  $RMSE$  to 32.9, and a reduction in  $MAE$  to 24.67. Incorporating the Gaussian MF (Gauss MF) significantly improves the model's accuracy, as evidenced by a decrease in  $RMSE$  to 31.35 and an increase in  $R^2$  to 0.41. The 4-4 Gauss MF configuration gives the best results, achieving the lowest  $RMSE$  of 30.14, the lowest  $MAE$  of 24.05, and the highest  $R^2$  value of 0.42, demonstrated in Figure 8.

Figure 8b displays the chart that compares two datasets: "trained" (red) and "original" (blue) across the same time or observation index. The original data exhibits high variability with frequent spikes, indicating the presence of extreme values or noise, while the trained model's output remains comparatively lower and more stable throughout.



**Fig. 8.** The result of satellite data using the Adaptive Neurofuzzy Inference System with Climate Hazards Group InfraRed Precipitation training phase: a) the root mean square error of training data, b) comparison chart of predicted results and actual data in training data; source: own study

### Validation phase

The performance evaluation of the model on the testing dataset under different configurations of membership functions is presented in Table 3. The evaluation metrics, including  $RMSE$ ,  $MAE$ , and  $R^2$ , provide insights into how these configurations influenced the model's ability.

The model was tested with different epochs (50 and 100) and two types of membership functions: Generalised Bell (Gbell MF) and Gaussian (Gauss MF). For 50 epochs using a 2-2 Gbell MF, the model achieved an  $RMSE$  of 33.3,  $MAE$  of 25.17, and an  $R^2$  of 0.37. When the number of epochs was increased to 100 with a 3-3 Gbell MF, the  $RMSE$  slightly decreased to 32.8,  $MAE$  to 24.62, while  $R^2$  remained similar at 0.36. The performance further improved when using Gaussian membership functions. With 100 epochs and 3-3 Gauss MF, the  $RMSE$  dropped to 31.31,  $MAE$  was

**Table 3.** Climate Hazards Group InfraRed Precipitation validation data performance with varying parameter

Epoch	MF	Shape	Training data		
			$RMSE$	$MAE$	$R^2$
50	2-2	Gbell MF	33.3	25.17	0.37
100	3-3	Gbell MF	32.8	24.62	0.36
100	3-3	Gauss MF	31.31	25.12	0.41
100	4-4	Gauss MF	30.14	24.05	0.42

Explanations as in Tab. 2.

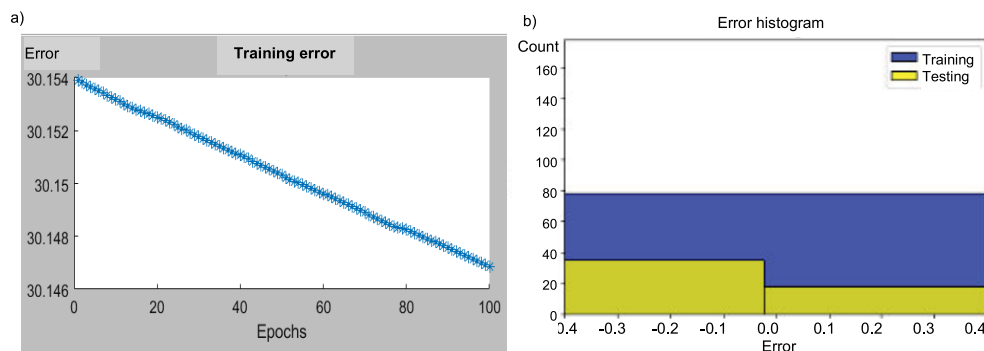
Source: own study.

25.12, and  $R^2$  increased to 0.41. The best performance was observed using 4-4 Gauss MF and 100 epochs, achieving an  $RMSE$  of 30.14,  $MAE$  of 24.05, and an  $R^2$  of 0.42. Figure 9 depicted the  $RMSE$  of training error for validation data and a comparison chart of predicted results versus actual data in the testing/validation data. Figure 9b indicates a histogram showing consistent performance between the training and testing phases, with most of the errors being small and centred around 0. The smaller frequency of testing errors (yellow) compared to training errors (blue) may be attributed to fewer testing samples or reduced variance.

### ANFIS training and validation result with ground station data

#### • Training phase

Table 4 presents the results of training the model using different number of epochs (50 and 100) and membership



**Fig. 9.** The result of the Adaptive Neurofuzzy Inference System training phase: a) the root mean square error of training data, b) comparison chart of predicted results and actual data in testing/validation data; source: own study



**Table 4.** Adaptive Neurofuzzy Inference System training performance with ground station data for different membership functions

Epoch	MF	Shape	Training data		
			RMSE	MAE	R <sup>2</sup>
50	2-2	Gbell MF	14.22	10.66	0.72
50	3-3	Gbell MF	8.3	6.64	0.73
50	3-3	Gauss MF	6.12	4.28	0.73
100	3.3	Gauss MF	6.05	3.63	0.74

Explanations as in Tab. 2.

Source: own study.

functions (MF), specifically Gbell MF and Gauss MF. With 50 epochs and a 2-2 Gbell MF configuration, the model achieved an *RMSE* of 14.22, an *MAE* of 10.66, and an *R*<sup>2</sup> of 0.72. Increasing the number of membership functions to a 3-3 Gbell MF while keeping the epochs at 50 resulted in a significant decrease in *RMSE* to 8.3 and *MAE* to 6.64, with a slight improvement in *R*<sup>2</sup> to 0.73. Switching to Gauss MF showed further improvement in the model's performance. Using 50 epochs and a 3-3 Gauss MF, the *RMSE* reduced further to 6.12, the *MAE* decreased to 4.28, and the *R*<sup>2</sup> remained at 0.73. Finally, increasing the number of epochs to 100 with 3-3 Gauss MF yielded the best results, achieving an *RMSE* of 6.05, an *MAE* of 3.63, and an *R*<sup>2</sup> value of 0.74. This indicates the model's enhanced ability to accurately fit the training data with this configuration.

#### • Validation phase

Table 5 presents the evaluation of the model's performance during the validation phase using validation data, under different configurations of epochs and MF. The evaluation metrics used include *RMSE*, *MAE*, and *R*<sup>2</sup>.

With a configuration of 50 epochs and 2-2 Gbell MF, the model achieved an *RMSE* of 14.11, an *MAE* of 10.65, and an *R*<sup>2</sup> of 0.72. Increasing the number of membership functions to 3-3 Gbell MF, with the same number of epochs, reduced the *RMSE* to 8.2, decreased the *MAE* to 6.60, and slightly improved the *R*<sup>2</sup> to 0.73. The use of Gauss MF yielded further enhanced performance. Using 50 epochs and 3-3 Gauss MF, the *RMSE* decreased to 6.1, the *MAE* to 4.21, while *R*<sup>2</sup> remained at 0.73. Finally, increasing the number of epochs to 100 with the 3-3 Gauss MF configuration resulted in the best performance, with an *RMSE* of 6.01,

**Table 5.** Adaptive Neurofuzzy Inference System validation performance using ground station data for different membership functions

Epoch	MF	Shape	Training data		
			RMSE	MAE	R <sup>2</sup>
50	2-2	Gbell MF	14.11	10.65	0.72
50	3-3	Gbell MF	8.2	6.60	0.73
50	3-3	Gauss MF	6.1	4.21	0.73
100	3.3	Gauss MF	6.01	3.60	0.74

Explanations as in Tab. 2.

Source: own study.

an *MAE* of 3.60, and an *R*<sup>2</sup> of 0.74. These results indicate an enhancement in model accuracy and an improved generalisation to validation data.

#### ANFIS-PCA training and validation result with ground station data

This process utilises the ANFIS-PCA algorithm, combining Adaptive Neuro-Fuzzy Inference System (ANFIS) with principal component analysis (PCA).

#### • Training phase

Table 6 summarises the training performance of the ANFIS-PCA model across different configurations of epochs and membership functions, evaluated using *RMSE*, *MAE*, and *R*<sup>2</sup> metrics. With 50 epochs and 2-2 Gbell MF, the model achieved an *RMSE* of 0.18, an *MAE* of 0.14, and an *R*<sup>2</sup> of 0.81. Increasing the number of epochs to 100 with the same membership function configuration slightly improved the *RMSE* to 0.17 and significantly reduced the *MAE* to 0.08, while *R*<sup>2</sup> remained consistent at 0.81. When using a configuration of 3-3 Gbell MF with 50 epochs, the model's performance improved further, achieving an *RMSE* of 0.16, an *MAE* of 0.12, and an *R*<sup>2</sup> of 0.82, suggesting a slightly better fit to the training data. Finally, with 100 epochs and 3-3 Gauss MF, the model achieved its best performance, yielding the lowest *RMSE* of 0.13, an *MAE* of 0.12, and an *R*<sup>2</sup> of 0.82, indicating enhanced accuracy in capturing the underlying patterns within the training dataset. Figure 10 illustrates two aspects of the ANFIS-PCA model's performance during training. The left panel presents the training error throughout the training epochs, while the right panel shows a comparison between the FIS output and the actual training data.

**Table 6.** Adaptive Neurofuzzy Inference System-principal component analysis training performance using ground station data

Epoch	MF	Shape	Training data		
			RMSE	MAE	R <sup>2</sup>
50	2-2	Gbell MF	0.18	0.14	0.81
100	2-2	Gbell MF	0.17	0.08	0.81
50	3-3	Gbell MF	0.16	0.12	0.82
100	3.3	Gauss MF	0.13	0.12	0.82

Explanations as in Tab. 2.

Source: own study.

The training error plot indicates the error trend over 100 epochs. The error, measured on the *y*-axis, starts at approximately 0.146 and gradually decreases throughout the training process, reaching about 0.137 by the final epoch. This indicates that the model is effectively learning and gradually minimising the discrepancy between predicted and actual values. Figure 10b displays the model's performance, where the trained model (red) performs reasonably well following the general trends of the original data (blue). However, it fails to capture the more extreme fluctuations.

#### • Validation phase

Table 7 presents the validation phase results for the ANFIS-PCA algorithm. The table summarises the model's performance under different configurations of epochs and MF, evaluated using metrics such as *RMSE*, *MAE*, and *R*<sup>2</sup>.

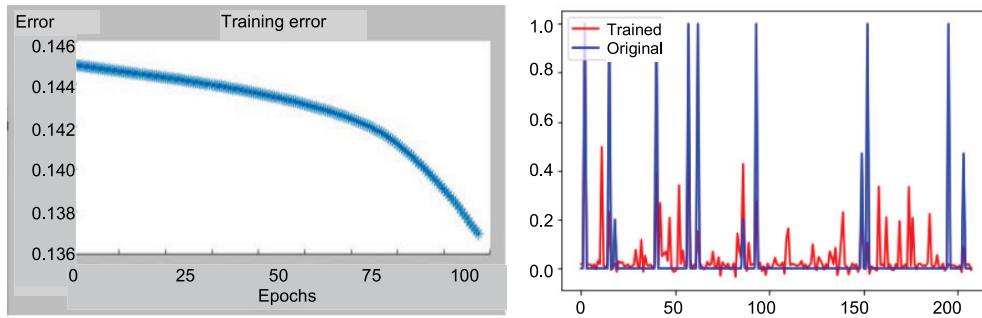


Fig. 10. Training error and model output comparison for Adaptive Neurofuzzy Inference System-principal component analysis model; source: own study

Table 7. Adaptive Neurofuzzy Inference System-principal component analysis validation performance using ground station data

Epoch	MF	Shape	Training data		
			RMSE	MAE	R <sup>2</sup>
50	2-2	Gbell MF	0.17	0.14	0.81
100	2-2	Gbell MF	0.16	0.12	0.81
50	3-3	Gbell MF	0.15	0.11	0.82
100	3.3	Gauss MF	0.12	0.10	0.82

Explanations as in Tab. 2.  
Source: own study.

With 50 epochs and a 2-2 Gbell MF, the model achieved an RMSE of 0.17, an MAE of 0.14, and an R<sup>2</sup> of 0.81. Increasing the number of epochs to 100 for the same membership function configuration resulted in an improvement, reducing the RMSE to 0.16 and the MAE to 0.12, while R<sup>2</sup> remained at 0.81. Using 50 epochs and 3-3 Gbell MF, the model further improved its performance, achieving an RMSE of 0.15, an MAE of 0.11, and an R<sup>2</sup> of 0.82. Finally, the best results were achieved with 100 epochs and 3-3 Gauss MF, attaining an RMSE of 0.12, an MAE of 0.10, and an R<sup>2</sup> of 0.82. Figure 11 illustrates the RMSE trend for training and validation errors, along with a comparison of predicted and actual data during testing/validation phases.

The histogram in Figure 11b displays the error distributions for the training (blue) and testing (yellow) phases of the model. Both distributions are centred around zero, indicating that the model generally produces small errors in both phases. The training data exhibits a higher frequency of errors tightly

clustered around zero, suggesting superior performance on the training set. In contrast, the testing errors are more dispersed, with a broader range, implying slightly reduced accuracy or generalisation when applied to unseen data. However, the overall concentration of both error distributions near zero indicates that the model performs reasonably well, with minimal bias or large prediction errors across both datasets.

### DISCUSSION

The present research investigates the critical role of data preprocessing and model selection in achieving reliable flood prediction. Through thorough data cleansing, the study eliminated anomalies such as missing, negative, or zero values, creating a robust foundation for model training. The performance of the ANFIS-PCA model during both training and validation phases, using two distinct data sources – ground station data and CHIRPS satellite data. The findings illustrate the significant impact that various factors, such as the number of epochs, the complexity of membership functions, and the integration of PCA, have on enhancing the model’s predictive accuracy. The study underscores the complementary strengths of the two data types used. Ground station data provides highly accurate, localised measurements, which lead to more precise learning and better performance metrics, as reflected by lower RMSE and MAE values. On the other hand, CHIRPS satellite data offers extensive spatial coverage, which helps the model capture broader rainfall patterns that may influence flooding events beyond the immediate vicinity of the ground stations. The integration of PCA was particularly impactful in reducing the dimensionality of the dataset, thereby facilitating a more efficient learning process by focusing on the most relevant features while minimising noise. By

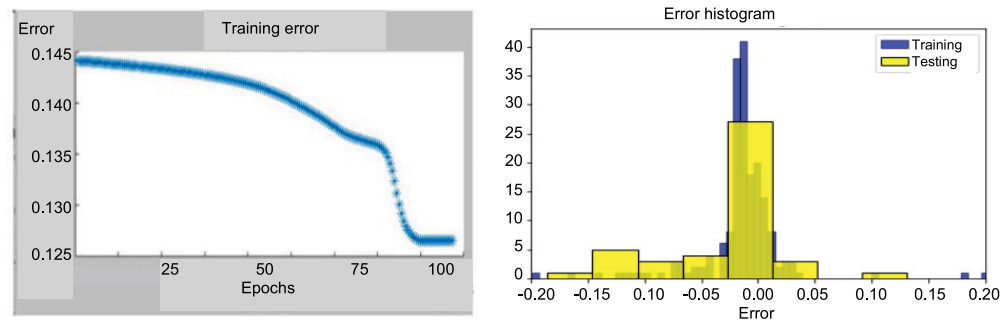


Fig. 11. The result of Adaptive Neurofuzzy Inference System-principal component analysis validation phase: a) the RMSE of training error of validation data, b) comparison chart of predicted results and actual data in testing/validation data; source: own study

applying PCA, the model concentrated on the key components that most strongly influenced flooding outcomes, which resulted in improved  $R^2$  values and reduced error metrics during both training and validation phases. The combination of PCA with ANFIS thus demonstrated a powerful approach for managing complex datasets, improving not only the accuracy but also the computational efficiency of the modelling process.

## CONCLUSIONS

This research establishes the Adaptive Neurofuzzy Inference System integrated with Principal Component Analysis (ANFIS-PCA) as a highly effective method for flood prediction, particularly when using ground station data for model training. The integration of PCA significantly improved the model's performance by focusing on key features and reducing noise, which contributed to lower *RMSE* and *MAE* values, along with higher  $R^2$  scores across both the training and validation phases. The increased accuracy achieved with Gaussian membership functions and the observed benefits of extending the number of training epochs further underscored the value of carefully tuning model parameters for optimal performance. Moreover, while ground station data enhanced model precision through detailed local insights, CHIRPS satellite data provided valuable regional perspectives, making it clear that a combined approach could lead to more robust flood prediction models. The findings suggest that the ANFIS-PCA model is well-suited for localised predictions, providing a reliable and accurate tool for predicting flooding events, while the broader scope offered by CHIRPS satellite data remains essential for capturing regional hydrological dynamics.

Future research could focus on integrating additional environmental variables input, such as water extent and soil moisture and flood conditioning factors like slopes, geomorphological units, land use, land cover, and soil physical properties, to further enhance predictive capability. The implementation of real-time dynamic learning could also be explored to adapt the model continuously as new data becomes available, thereby enhancing the reliability of real-world flood prediction systems. Additionally, comparing ANFIS-PCA with advanced deep learning techniques, such as long short-term memory and random forest, could provide insights into the competitiveness of different approaches for capturing complex spatiotemporal patterns. The authors suggest implementing bias correction in future stages of the research. Bias correction methods can significantly improve model reliability by adjusting systematic discrepancies between observed and predicted data. Additionally, the authors propose the use of quantile-mapping correction or non-parametric bias correction. This method is particularly effective in addressing differences in distribution between the observed data and the modelled data, thereby ensuring that the predicted outputs better reflect the statistical properties of the actual data.

## ABBREVIATIONS

ANFIS	Adaptive Neuro-Fuzzy Inference System
AI	artificial intelligence
ANN	artificial neural network
ARG	automatic rain gauge

CHIRPS	Climate Hazard Group Infrared Precipitation with Station
<i>IQR</i>	interquartile range
<i>MAE</i>	mean absolute error
NN	neural network
PCA	principal component analysis
Q1	first quartile
Q2	second quartile
Q3	third quartile
$R^2$	coefficient of determination
<i>RMSE</i>	root mean square error
SVM	support vector machine
SVR	support vector regression

## ACKNOWLEDGMENTS

Gratitude is extended to STMKG (Sekolah Tinggi Meteorologi Klimatologi dan Geofisika) for their invaluable support in the research conducted in Bogor-Jakarta, Indonesia. The financial assistance provided for the publication of this article is deeply appreciated. Special acknowledgement is given to the Education and Training Center BMKG for their funding support through the research groups.

## CONFLICT OF INTERESTS

All authors declare that they have no conflict of interests.

## REFERENCES

- Ahmadi, N. and Moradina, S.F. (2024) "An approach for flood flow prediction utilizing new hybrids of ANFIS with several optimization techniques: A case study," *Hydrology Research*, 55(5), pp. 560–575. Available at: <https://doi.org/10.2166/nh.2024.191>.
- Al-Areeq, A.M. *et al.* (2024) "Implication of novel hybrid machine learning model for flood subsidence susceptibility mapping: A representative case study in Saudi Arabia," *Journal of Hydrology*, 630, 130692. Available at: <https://doi.org/10.1016/j.jhydrol.2024.130692>.
- Amiri, A. *et al.* (2024) "A novel machine learning tool for current and future flood susceptibility mapping by integrating remote sensing and geographic information systems," *Journal of Hydrology*, 632, 130936. Available at: <https://doi.org/10.1016/j.jhydrol.2024.130936>.
- Ansari, S. *et al.* (2021) "Parameter tuning of MLP, RBF, and ANFIS models using genetic algorithm in modeling and classification applications," *2021 International Conference on Information Technology, ICIT 2021*, Amman, Jordan 14–15 July 2021. Amman: Al-Zaytoonah University of Jordan, pp. 660–666. Available at: <https://doi.org/10.1109/ICIT52682.2021.9491682>.
- Antzoulatos, G. *et al.* (2022) "Flood hazard and risk mapping by applying an explainable machine learning framework using satellite imagery and GIS data," *Sustainability*, 14(6), 3251. Available at: <https://doi.org/10.3390/su14063251>.
- Arora, A. *et al.* (2021) "Optimization of state-of-the-art fuzzy-metaheuristic ANFIS-based machine learning models for flood susceptibility prediction mapping in the Middle Ganga Plain, India," *Science of the Total Environment*, 750, 141565. Available at: <https://doi.org/10.1016/j.scitotenv.2020.141565>.

- Bennett, W.G. *et al.* (2023) "Modelling compound flooding: A case study from Jakarta, Indonesia." *Natural Hazards*, 118(1), 277–305. Available at: <https://doi.org/10.1007/s11069-023-06001-1>.
- Bensaid, R. *et al.* (2024) "Toward a real-time TCP SYN flood DDoS mitigation using adaptive neuro-fuzzy classifier and SDN assistance in fog computing." *Security and Communication Networks*, 2024, 651584. Available at: <https://doi.org/10.1155/2024/6651584>.
- Buuren van, S. and Groothuis-Oudshoorn, K. (2011) "mice: Multi-variate Imputation by Chained Equations in R." *Journal of Statistical Software*, 45(3), pp. 1–67. Available at: <https://doi.org/10.18637/jss.v045.i03>.
- Cho, I., Park, S. and Kim, J. (2022). "A fire risk assessment method for high-capacity battery packs using interquartile range filter." *Journal of Energy Storage*, 50, 104663. Available at: <https://doi.org/10.1016/j.est.2022.104663>.
- Dong, S. *et al.* (2021) "A hybrid deep learning model for predictive flood warning and situation awareness using channel network sensors data." *Computer-Aided Civil and Infrastructure Engineering*, 36(4), pp. 402–420. Available at: <https://doi.org/10.1111/mice.12629>.
- Du, H. *et al.* (2024) "Evaluating the effectiveness of CHIRPS data for hydroclimatic studies." *Theoretical and Applied Climatology*, 155(3), pp. 1519–1539. Available at: <https://doi.org/10.1007/s00704-023-04721-9>.
- Gabr, M.I., Helmy, Y.M. and Elzanfaly, D.S. (2023) "Effect of missing data types and imputation methods on supervised classifiers: An evaluation study." *Big Data and Cognitive Computing*, 7(1), 55. Available at: <https://doi.org/10.3390/bdcc7010055>.
- García-Laencina, P.J., Sancho-Gómez, J.L. and Figueiras-Vidal, A.R. (2010) "Pattern classification with missing data: A review." *Neural Computing and Applications*, 19(2), pp. 263–282. Available at: <https://doi.org/10.1007/s00521-009-0295-6>.
- Günal, A.Y. (2024) "Implementing fuzzy SMRGT, ANN, and ANFIS for flow coefficient estimation in Antalya River Basin." *Journal of Hidrology*, 640, 131705. Available at: <https://doi.org/10.1016/j.jhydrol.2024.131705>.
- Hassan, W.I., Joseph, I. and Abubakar, S. (2024) "Assessment of effect of flooding and flood risk reduction strategies in urban centres." *Journal of Built Environment and Geological Research*, 04(4), pp. 286–299. Available at: <https://africanscholarpub.com/ajbegr/article/view/231/238> (Accessed: June 03, 2024).
- Helmi, A.M. *et al.* (2024) "Comparing remote sensing and geostatistical techniques in filling gaps in rain gauge records and generating multi-return period isohyetal maps in arid regions – Case study: Kingdom of Saudi Arabia." *Water*, 16(7), 925. Available at: <https://doi.org/10.3390/w16070925>.
- Indriastuti, D. (2016) "Analysis of runoff due to the change in land use at the watershed of Upstream Ciliwung." *Journal of the Civil Engineering Forum*, 2(1), 131. Available at: <https://doi.org/10.22146/jcef.26576>.
- Islam, A.R.M.T. *et al.* (2023) "Improvement of flood susceptibility mapping by introducing hybrid ensemble learning algorithms and high-resolution satellite imageries." *Natural Hazards*, 119(1), pp. 1–37. Available at: <https://doi.org/10.1007/s11069-023-06106-7>.
- Jang, J.-R.R. (1993) "ANFIS: Adaptive-network-based fuzzy inference system." *IEEE Transactions on Systems, Man, and Cybernetics*, 23(3), pp. 665–685. Available at: <https://doi.org/10.1109/21.256541>.
- Karamizadeh, S. *et al.* (2013) "An overview of Principal Component Analysis." *Journal of Signal and Information Processing*, 04(3B), pp. 173–175. Available at: <https://doi.org/10.4236/jsip.2013.43b031>.
- Llovo, I.F., Mosqueira, J. and Vidal, F. (2018) "Analysis of the Mean Absolute Error (MAE) and the Root Mean Square Error (RMSE) in Assessing Rounding Model Analysis of the Mean Absolute Error (MAE) and the Root Mean Square Error (RMSE) in Assessing Rounding Model." *OP Conference Series: Materials Science and Engineering*. Available at: <https://doi.org/10.1088/1757-899X/324/1/012049>.
- Ly H.-B. *et al.* (2019) "Improvement of ANFIS model for prediction of compressive strength of manufactured sand concrete." *Applied Sciences*, 9(18), 3841. Available at: <https://doi.org/10.3390/app9183841>.
- Maharana, K., Mondal, S. and Nemade, B. (2022) "A review: Data preprocessing and data augmentation techniques." *Global Transitions Proceedings*, 3(1), pp. 91–99. Available at: <https://doi.org/10.1016/j.gltp.2022.04.020>.
- Navale, V. and Mhaske, S. (2023) "Artificial Neural Network (ANN) and Adaptive Neuro-Fuzzy Inference System (ANFIS) model for forecasting groundwater level in the Pravara River Basin, India." *Modeling Earth Systems and Environment*, 9(2), pp. 2663–2676. Available at: <https://doi.org/10.1007/s40808-022-01639-5>.
- Pishnamazi, M. *et al.* (2020) "ANFIS grid partition framework with difference between two sigmoidal membership functions structure for validation of nanofluid flow." *Scientific Reports*, 10, 15395. Available at: <https://doi.org/10.1038/s41598-020-72182-5>.
- Priyambodoho, B.A. *et al.* (2021) "Flood inundation simulations based on GSMAp satellite rainfall data in Jakarta, Indonesia." *Progress in Earth and Planetary Science*, 8, 34. Available at: <https://doi.org/10.1186/s40645-021-00425-8>.
- Rachmawardani, A. *et al.* (2022) "State of the art of remote sensing in flood early warning system: review article." *Social, Humanities, and Educational Studies (SHES): Conference Series*, 5(4), 108. Available at: <https://doi.org/10.20961/shes.v5i4.68977>.
- Rashidi Shikhteymour, S. *et al.* (2023) "A novel approach for assessing flood risk with machine learning and multi-criteria decision-making methods." *Applied Geography*, 158, 103035. Available at: <https://doi.org/10.1016/j.apgeog.2023.103035>.
- Rudra, R.R. and Sarkar, S.K. (2023) "Artificial neural network for flood susceptibility mapping in Bangladesh." *Heliyon*, 9(6), e16459. Available at: <https://doi.org/10.1016/j.heliyon.2023.e16459>.
- Sahoo, A., Samantaray, S. and Paul, S. (2021) "Efficacy of ANFIS-GOA technique in flood prediction: A case study of Mahanadi River basin in India." *H2Open Journal*, 4(1), pp. 137–156. Available at: <https://doi.org/10.2166/H2OJ.2021.090>.
- Samantaray, S. *et al.* (2023) "Flood discharge prediction using improved ANFIS model combined with hybrid particle swarm optimisation and slime mould algorithm." *Environmental Science and Pollution Research*, 30, pp. 83845–83872. Available at: <https://doi.org/10.1007/s11356-023-27844-y>.
- Santos, L.B.L. *et al.* (2023) "A neural network-based hydrological model for very high-resolution forecasting using weather radar data." *Eng*, 4(3), pp. 1787–1796. Available at: <https://doi.org/10.3390/eng4030101>.
- Saridewi, T.R. and Fauzi, A. (2019) "A market-based mechanism as an alternative solution for watershed management: a case study of the Ciliwung Watershed, Indonesia." *International Journal of Global Environmental Issues*, 18(2), 171. Available at: <https://doi.org/10.1504/ijgenvi.2019.10023932>.
- Sarkar, S.C. *et al.* (2021) "Application of soft computing for time series water-level prediction in Jamuna River." *International Journal of Systematic Innovation*, 6(6), pp. 13–21. Available at: [https://doi.org/10.6977/IJoSI.202112\\_6\(6\).0003](https://doi.org/10.6977/IJoSI.202112_6(6).0003).

- Shabbir, J. and Ahmed, A. (2022) "Computation estimation of interquartile range in stratified sampling under non-linear cost function," *Communications in Statistics – Simulation and Computation*, 51(4), pp. 1891–1898. Available at: <https://doi.org/10.1080/03610918.2019.1689267>.
- Shahid, M. *et al.* (2021) "Assessing the potential and hydrological usefulness of the CHIRPS precipitation dataset over a complex topography in Pakistan," *Hydrological Sciences Journal*, 66(11), pp. 1664–1684. Available at: <https://doi.org/10.1080/02626667.2021.1957476>.
- Singh, D. and Singh, B. (2020) "Investigating the impact of data normalization on classification performance," *Applied Soft Computing*, 97(B), 105524. Available at: <https://doi.org/10.1016/j.asoc.2019.105524>.
- Srilakshmi, K. *et al.* (2024) "Optimization of ANFIS controller for solar/battery sources fed UPQC using an hybrid algorithm," *Electrical Engineering*, 106(4), pp. 3743–3770. Available at: <https://doi.org/10.1007/s00202-023-02185-8>.
- Sulugodu, B. and Deka, P.C. (2019) "Evaluating the performance of CHIRPS satellite rainfall data for streamflow forecasting," *Water Resources Management*, 33(11), pp. 3913–3927. Available at: <https://doi.org/10.1007/s11269-019-02340-6>.
- Szeląg, B. *et al.* (2024) "Tool for fast assessment of stormwater flood volumes for urban catchment: A machine learning approach," *Journal of Environmental Management*, 355, 120214. Available at: <https://doi.org/10.1016/j.jenvman.2024.120214>.
- Wang, M. *et al.* (2021) "Sourcing CHIRPS precipitation data for streamflow forecasting using intrinsic time-scale decomposition based machine learning models," *Hydrological Sciences Journal*, 66(9), pp. 1437–1456. Available at: <https://doi.org/10.1080/02626667.2021.1928138>.
- Youssef, A.M. *et al.* (2023) "Flood vulnerability mapping and urban sprawl suitability using FR, LR, and SVM models," *Environmental Science and Pollution Research*, 30(6), pp. 16081–16105. Available at: <https://doi.org/10.1007/s11356-022-23140-3>.
- Zein, M.R., Anggraheni, E. and Yahya, D.M. (2023) "Impact analysis of land use changes on inundation map in The Ciliwung River Watershed," *CSID Journal of Infrastructure Development*, 6(2), 3. Available at: <https://doi.org/10.7454/jid.v6.i2.1117>.